Modeling of High-Performance SPR Refractive Index Sensor Employing Novel 2D Materials for Detection of Malaria Pathogens

Abinash Panda and Puspa Devi Pukhrambam, *Member, IEEE*

***Abstract*— The present work exhibits a novel design of surface plasmon resonance (SPR) biosensor, which comprises CaF_2 prism, TiO_2, metal (Ag/Au), $PtSe_2$, 2D materials (graphene/transition metal dichalcogenides (MoS_2/WS_2)) and sensing medium, for point-of-care detection of various stages of malaria diseases. The transfer matrix method (TMM) is employed to examine the angular reflectivity of the proposed structure after judiciously optimizing the layer thicknesses and layer numbers. Phase interrogation technique is utilised to validate the position of occurrence of resonance angles. Additionally, the proposed SPR structure is designed using COMSOL Multiphysics, to assay the electric field intensity and electric field enhancement factor near the edge of 2D material-sensing layer interface. Simulation upshots revealed that the use of new class of 2D materials catapult the sensor performance to a new height compared to the traditional SPR configuration. A maximum sensitivity of 240.10 °/RIU, quality factor of 78.46 RIU^{-1} and detection accuracy of 1.99 is attained for Ag-based SPR configuration with bilayer of WS_2. Sensing parameters are compared with previously reported works to prove the superiority of the present research. Moreover, the real-time and label-free detection of malaria diseases makes the suggested sensor worth to fabricate as a SPR chip with the recent nanofabrication technologies.**

***Index Terms*— Surface plasmon resonance, 2D materials, biosensor, transfer matrix method, sensor performance, electric field intensity enhancement factor.**

I. Introduction

SPR technology has developed as a magnificent method for label-free and real-time detection of various biomolecules with minute refractive index (RI) contrast [1]. SPR methodology has seen a sharp increase in demand in recent years for their wide range of applications such as environment monitoring [2], liquid level sensing, food safety [3], pressure and temperature monitoring [4], medical diagnostics [5]. SPR phenomenon gives rise to evanescent wave at the interface of positive and negative permittivity materials [6]. When the frequency of the evanescent wave matches with the natural frequency of surface plasmon wave (SPW), appropriate SPR condition is entrenched. SPR computes the resonance angle, which is formed in the reflectance characteristics, where a sharp fall in the reflection spectrum is accomplished on the total transformation of energy from evanescent wave to SPW. Any feeble alteration in the RI of the sensing medium induces a substantial change in the resonance angle and that makes the SPR an ultrasensitive technique for detection of wide range of analytes. Mostly, Kretschmann configuration is employed to envisage SPR characteristics, where a thin film of metal (gold and silver) with a thickness of 40-50 nm is deposited on a prism [7], [8]. Gold (Au) is recommended as a suitable noble metal in SPR configuration, owing to its high corrosion resistance. Au shows high operational stability and high sensitivity, which makes it an ultimate choice for liquid sensing. On the contrary, silver (Ag) film shows finer resonance peak, which enhances the detection accuracy, but conveys lower sensitivity [9]. Apart from Au and Ag, recently researchers have shown faith on some additional metals such as aluminium and copper for generation of surface plasmon waves [10], [11], but they suffer easy oxidation and require other protection layers, which makes the design more bulky. To enhance the sensing performances of traditional Kretschmann configuration based SPR sensor, noble 2D nanomaterials such as graphene, $MoSe_2$, WS_2, $PtSe_2$ can be utilised on the metal layer [12], [13]. These 2D materials can significantly improve the absorption of various analytes present in the sensing medium.

Graphene has gained considerable response on electromagnetic applications because of its supreme features, for instance, robustness, high mobility, single atom thickness, flexibility, durability, unmatched optical, thermal and noteworthy conductivity at room temperature, frequency-independent absorption of EM radiation, electronic energy spectrum [14], [15]. Being a low noise, feeble loss and zero-gap semiconductor material, graphene has come up as an apt aspirant for sensing of light weight molecules near its surface [16]. Aside from graphene, other novel 2D materials such as WS_2 and $MoSe_2$ have developed as the most apt substitute for envisaging SPR based sensors. These materials belong to the Transition metal dichalcogenides (TMDC) group and they have appealed a significant research heed owing to their scalability property, and thickness dependent optical properties. WS_2 and MoS_2 has large band gap of 1.94eV and 1.77eV respectively, which is higher than many conventional semiconductor like GaAs, InAs, InN, InP, InSb etc., thus make them possible to operate at a high temperature and voltage. With a broad work function of 5.1eV, MoS_2 and WS_2 offer high affinity surface area to absorb the bio-analytes and thus utilized in bio-sensing

Manuscript received July 20, 2021; revised September 7, 2021; accepted September 23, 2021. Date of publication September 27, 2021; date of current version April 1, 2022. *(Corresponding author: Abinash Panda.)*

The authors are with the Department of Electronics and Communication Engineering, National Institute of Technology, Silchar, Assam 788010, India (e-mail: abinashpanda087@gmail.com; puspa.devi@ece.nits.ac.in).

Digital Object Identifier 10.1109/TNB.2021.3115906

applications. Moreover, the high photoluminescence, non-blinking photon emission, wider PBG (photonic band gap), high spin orbit coupling of 420meV, make these 2D materials as a favourable option to realize biosensors [17], [18]. Recently, $PtSe_2$ has come up as a wonderful candidate for numerous photonics applications because of its unparalleled electrical and optical properties, and adjustable bandgap in the range 1.2eV to 0.21eV [19]. Additionally, $PtSe_2$ shows high inertness towards several chemical agents and offers commendable resistance to toxic effect, which makes it an apposite contender for bio-sensing applications [20]. Despite of the noteworthy properties of 2D materials compared to the conventional bulk materials, it is quiet challenging to control the thickness of the 2D materials during their large-scale development. Recently, scientist have successfully fabricated thickness controlled 2D materials with high scalability by employing different cutting edge techniques such as Chemical Vapour Deposition (CVD) and mechanical exfoliation method, metal-organic CVD and atomic layer deposition (ALD) method [21]–[24].

Kumar *et al.* theoretically analyzed a Kretschmann configuration based SPR design containing BK7/ZnO/Ag/$BaTiO_3$/WS_2, which delivers a maximum sensitivity of 235°/RIU and quality factor of 63.51RIU^{-1} [25]. Moznuzzaman *et al.* performed a detailed theoretical investigation of a SPR sensor with configuration SF11/Ag/graphene/MoS2/TiO2/SiO2 for detection of formalin concentrations with a sensitivity of 98 °/RIU and detection accuracy of 0.88 [26]. Devi *et al.* [27] performed numerical simulations to obtain different sensing characteristics of SPR by employing 2D materials like graphene, WSe_2, GO and MoS_2, where the authors obtained a sensitivity of 151.8 °/RIU and detection accuracy of 0.22 degree^{-1} but they have not performed the electric field analysis in the structure. Kumar *et al.* [28] theoretically investigated BK7/ZnO/Ag/Au/Graphene configuration based SPR biosensor and achieved a maximum sensitivity of 66 degree/RIU with monolayer of graphene at 632.8 nm. Panda *et al.* [29] reported a theoretical study of graphene coated SPR sensor to detect both liquid and gaseous analytes. Wang *et al.* [30] theoretically demonstrated a SPR sensor consisting of graphene, WS_2 and Au/Ag bimetallic layer, where thickness of Au/Ag and no. of layers of graphene/WS_2 are suitably optimized and the authors concluded that single layer of graphene/WS_2 delivers maximum sensitivity. A SPR based biosensor is presented theoretically, which employs Si and 2D MXene (Ti_3C_2Tx) to increase the angular sensitivity [31]. Sreekanth *et al.* fabricated and experimentally characterized a highly sensitive plasmonic sensor designed with hyperbolic metamaterials (HMMs) [32]–[34]. They explored the unusual and unique properties of HMMs and analysed the spectral properties of the sensor in visible to NIR wavelength regime. Kabashin *et al.* demonstrated an improved SPR biosensor by fabricating a new kind of plasmonic metamaterial [35]. Garoli *et al.* fabricated nanoporous gold (NPG) film based SPR sensor to detect a wide range of biomolecules, where the authors achieved a notably high sensitivity of 15000 nm/RIU in the NIR regime [36]. Calandrini *et al.* performed an experimental analysis of sensing performance of a NPG based plasmonic resonator and compared the outcomes with analogous structure designed with homogeneous gold [37]. The authors attained a remarkable sensitivity of more than 4000 nm/RIU.

TABLE I
REFRACTIVE INDEX OF RBC FOR DIFFERENT STAGES OF MALARIA INFECTION [40]

Malaria different stage	Refractive index
Normal stage	1.408
Ring stage	1.396
Trophozoite stage	1.381
Schizont stage	1.371

Malaria disease, which is spread by infected female Anopheles mosquitoes, has become the global concern owing to its adverse health effect, which may also leads to death. According to a recent report of World Health Organization, 228 million cases of malaria were recorded in 2018 worldwide, out of which 405,000 number of deaths were reported [38]. If malaria is not diagnosed early, then it becomes difficult to cure the disease [39]. The optical properties of RBC (red blood cell) present in the blood plays a key role in determination of different stages of malaria diseases. In the malaria infected RBCs, it is found that the parasite plasmodium falciparum is unevenly multiplied, which leads to different stages of malaria infection such as ring, trophozoite, and schizont stage. Hemoglobin and water are the prime constituents of RBC, so any small variations in hemoglobin concentrations leads to change in the refractive index of RBC. Higher infected cell results in decrement of hemoglobin content, which modifies the refractive index of RBC. The refractive index of RBC for different stages of malaria infection is listed in Table I.

The present research has couple of newness such as complete structural optimization is performed vis-à-vis various layer thicknesses and layer numbers by separately considering Au and Ag as the metal layer. Sensor performances are assayed by discretely coating various novel 2D materials like graphene/MoS2/WS2 beneath the sensing layer. Both the transfer matrix method (TMM) and angular interrogation technique are employed to examine the reflectivity and validate the position of resonance angle. The proposed sensor is also modelled and simulated in COMSOL Multiphysics environment, where a detailed assay of electric field intensity and field enhancement factor are carried out in the vicinity of 2D material-sensing layer interface, which further boosts the novelty of the present work. On top of that, compared to the conventional sensor configuration, which emphases on enhancement of performance parameters only, the present research deals with the investigation of several physical quantities. Besides this, we compared the sensor performance with some recently published theoretical works to prove the superiority of this research.

II. SENSOR DESIGN AND NUMERICAL ANALYSIS

The present research is grounded on Kretschmann based SPR structure, which contains six layers: CaF2 prism, TiO2 adhesion, metal (Ag/Au), PtSe2, 2D materials (graphene/MoS2/WS2) and sensing layer, and the same is delineated in Fig. 1. The He-Ne laser is used to generate p-polarized light of wavelength 632.8 nm. Here, a CaF_2

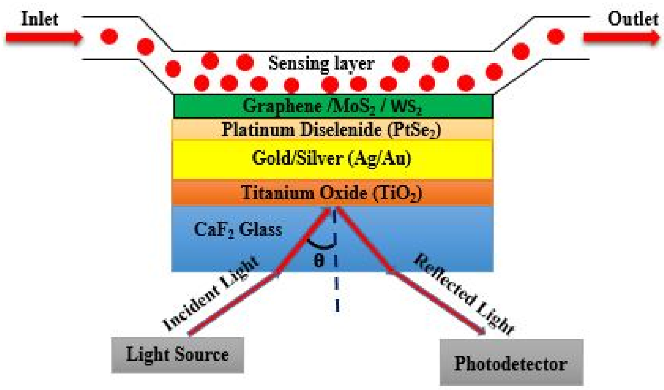

Fig. 1. Structural arrangement of the proposed SPR biosensor with full setup.

glass of 1000 nm thickness is employed as the coupling prism. A thin layer of TiO2 with a thickness of 10 nm can be coated above the prism surface by using sputtering method [41]. TiO_2 acts as an adhesion layer, which assures a strong contact between prism and metal layer. A metal layer (Ag/Au) having optimized thickness of 45 nm can be grown on the TiO_2 layer by following high power impulse magnetron sputtering method [42]. A thin layer of $PtSe_2$ with a thickness of 4nm can be coated over the metal surface by spin coating technique. Further, graphene, MoS_2 and WS_2 layers of different thicknesses can be grown separately by chemical vapour deposition technique [23], [24]. Moreover, the optical properties of these 2D materials can be controlled by judiciously selecting their thickness. Therefore, in fabrication process, outmost care must be taken to control the thickness of the 2D materials. The last layer is referred as the sensing layer, where blood cells (biorecognition element) are infiltrated for detection and diagnosis of malaria diseases. The physical parameters of different layers are summarized in the Table II.

At a wavelength (λ) of 632.8 nm, the RI of CaF_2 based prism layer and TiO_2 adhesion layer can be computed through the following Sellmeier equations [43],

$$n_{CaF_2} = \sqrt{\begin{array}{l} 1+\dfrac{0.567888\lambda^2}{\lambda^2-0.0502636^2}+\dfrac{0.471091\lambda^2}{\lambda^2-0.100390^2} \\ +\dfrac{3.848472\lambda^2}{\lambda^2-34.649040^2} \end{array}} \quad (1)$$

$$n_{TiO_2} = \sqrt{5.913+\frac{0.2441}{\lambda^2-0.0803}} \quad (2)$$

The refractive index of Ag and Au at the operating wavelength (λ) is attained by using Drude model [44],

$$n_{Ag} = \sqrt{1-\frac{\gamma_e\lambda^2}{\gamma_p^2(\gamma_e+i\lambda)}} = \sqrt{1-\frac{17.614\lambda^2}{0.1454^2(17.614+i\lambda)}} \quad (3)$$

$$n_{Au} = \sqrt{1-\frac{\gamma_e\lambda^2}{\gamma_p^2(\gamma_e+i\lambda)}} = \sqrt{1-\frac{8.934\lambda^2}{0.1682^2(8.934+i\lambda)}} \quad (4)$$

where, γ_e and γ_p denote the collision wavelength and plasma wavelength respectively. The RI of graphene layer at 632.8 nm is computed by the following expression [28],

$$n_{graphene} = 3+i\frac{C_1}{3}\lambda \quad (5)$$

TABLE II
REFRACTIVE INDEX AND OPTIMIZED THICKNESS OF DIFFERENT LAYERS OF THE PROPOSED STRUCTURE

Different layers	Material used	Refractive index	Thickness (nm)
Layer 1	CaF_2	1.4329	1000
Layer 2	TiO_2	1.99	10
Layer 3	Ag	0.135+3.985i	45
	Au	0.181+3.068i	45
Layer 4	PtSe2	2.916+1.298i	4
Layer 5	graphene (monolayer)	3+1.149i	0.34
	MoS_2 (monolayer)	5.08+1.172i	0.65
	WS_2 (monolayer)	4.9+0.312i	0.80
Layer 6	Analyte	Refer table 1	400

where, the constant C_1 takes the value of 5.446 μm^{-1}. The RI of other layers consisting of TMDC materials are collected from the [13]. The multi-Lorentzian function is employed to acquire the dielectric function of MoS_2 and WS_2, which can be specified as [45],

$$\varepsilon(E) = 1+\sum_{k=1}^{N}\frac{f_k}{E_k^2-E^2-iE\rho_k} \quad (6)$$

where, E indicates the energy of the photon particle, which is expressed as $(eV) = \frac{1.2398}{\lambda(\mu m)}$, the model parameters f_k, E_k and ρ_k signify the oscillation strength, resonance energy and spectral width of k^{th} oscillation respectively and their values can be computed from the experimental data presented in the [46].

The reflectivity of the light from the proposed N-layer structure is computed by employing transfer matrix method (TMM). The layers are arranged along the z-direction as depicted in Fig. 2. The relationship between the tangential field components of the first and final boundary can be expressed mathematically as follows [8],

$$\begin{bmatrix} E_1 \\ H_1 \end{bmatrix} = M \begin{bmatrix} E_{N-1} \\ H_{N-1} \end{bmatrix} \quad (7)$$

where, E_1 and E_{N-1} denote the tangential electric field components at the boundary of the first layer and N^{th} layer respectively. Similarly, H_1 and H_{N-1} signify the tangential magnetic field components at the boundary of the first layer and N^{th} layer respectively. M_{ij} represents the elements of the characteristics matrix M, which is stated as [9],

$$M_{ij} = \left(\prod_{s=2}^{N-1} M_s\right)_{ij} = \begin{pmatrix} M_{11} & M_{12} \\ M_{21} & M_{22} \end{pmatrix} \quad (8)$$

$$M_s = \begin{pmatrix} cos\beta_s & -(isin\beta_s)/q_s \\ -iq_s sin\beta_s & cos\beta_s \end{pmatrix} \quad (9)$$

where,

$$q_s = \sqrt{\frac{\mu_s}{\varepsilon_s}}cos\theta_s = \frac{\left(\varepsilon_s-n_1^2sin^2\theta_1\right)^{\frac{1}{2}}}{\varepsilon_s} \quad (10)$$

And

$$\beta_s = \frac{2\pi d_s}{\lambda}\left(\varepsilon_s-n_1^2sin^2\theta_1\right)^{1/2} \quad (11)$$

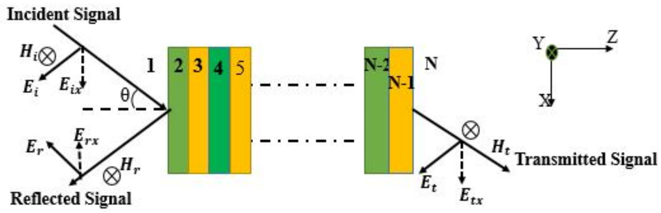

Fig. 2. Layer arrangement of the proposed structure.

In equation (11), θ_1 represents the incident angle at the CaF_2 glass prism, λ is the operating wavelength. The symbols ε_s and d_s denote the dielectric constant and thickness of s^{th} layer respectively. It is to be noted that for 2D materials, the value of ε_s and d_s depend on the number of layers. By using equation (9), transfer matrix of each layer is computed. Finally, the transfer matrix of the entire N-layer structure is evaluated by multiplying the transfer matrix of individual layers [28]. The reflection intensity (R_p) is calculated by using the matrix elements as follows [12],

$$R_p = \left| \frac{(M_{11} + M_{12}q_N)q_1 - (M_{21} + M_{22}q_N)}{(M_{11} + M_{12}q_N)q_1 + (M_{21} + M_{22}q_N)} \right|^2 \quad (12)$$

A. Performance Measuring Parameters

Sensitivity, quality factor and detection accuracy are considered as the most important sensing parameters to judge the performance of a sensor [28], [29]. The angular sensitivity (S_θ) is described as the ratio of change in the SPR angle ($\Delta\theta_{res}$) to the variation in analyte RI (Δn), which can be expressed as below,

$$S_\theta(^\circ/RIU) = \frac{\Delta\theta_{res}}{\Delta n} \quad (13)$$

The quality factor (Q) is measured through dividing angular sensitivity by full width half maximum (FWHM) of the SPR curve, which is expressed as,

$$Q(RIU^{-1}) = \frac{S_\theta}{FWHM} \quad (14)$$

Detection accuracy (DA) is computed as the ratio of $\Delta\theta_{res}$ and FWHM, which can be given as,

$$DA = \frac{\Delta\theta_{res}}{FWHM} \quad (15)$$

III. Results and Analysis

As per the law of energy conversion, the signal undergoes three different phenomenon namely absorption (A), transmission (T) and reflection (R) such that A+T+R=1. The incident light cannot transmit through the proposed Kretschmann structure i.e. T=0, so A+R=1. Thus, if reflectance becomes minimum, then more amount of light will be absorbed in the structure, which enhances the light matter interaction and sensitivity.

We evaluated the sensor performance by selecting two different materials Au and Ag as the metal layer. Fig. 3 depicts the reflectance curves with respect to incident angle for a variation in the metal layer thickness from 25 nm to 65 nm with an interval of 10 nm. It can be observed that for both Ag and Au, minimum reflectivity is attained at the resonance

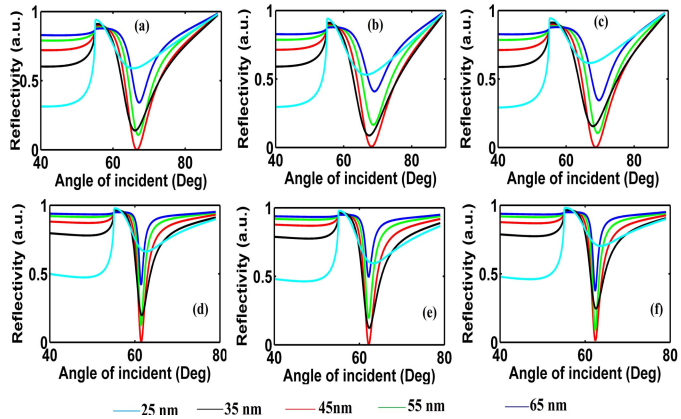

Fig. 3. Optimization of thickness of metal layer (a) Au+ $PtSe_2$+graphene (b) Au+ $PtSe_2$+ MoS_2 (c) Au+ $PtSe_2$+ WS_2 (d) Ag+ $PtSe_2$+graphene (e) Ag+ $PtSe_2$+ MoS_2 (f) Ag+ $PtSe_2$+ WS_2.

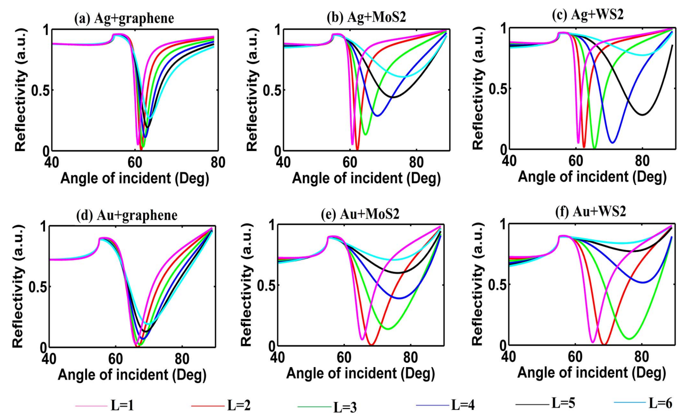

Fig. 4. Variation in the number of layers (L) of graphene/MoS_2/WS_2 in the proposed configurations.

condition for the thickness of 45 nm. So, for maximum sensing performance, the optimized thickness of the metal layer is considered to be 45 nm.

Fig. 4 displays the impact of number of layers (L) of graphene, MoS_2 and WS_2 on the SPR characteristics with fixed $PtSe_2$ thickness of 4 nm and Ag/Au thickness of 45 nm. It is perceived that minimum reflectivity is obtained for L=1 in all cases except for Ag+ WS_2 configuration (fig. 4 (c)), where the reflectance tends to zero for L=2. It is clearly observed that with increase in L of graphene/MoS_2/WS_2, the reflected intensity increases and the SPR curves become broaden with higher FWHM (full width half maximum). Owing to the higher values of FWHM, the sensor performance degrades and it becomes difficult for practical realization of the device. So, monolayer (L=1) is the best choice for CaF_2+Au+$PtSe_2$+graphene/MoS_2/WS_2 and CaF_2+Ag+ $PtSe_2$+graphene/MoS_2 based design, whereas bilayer (L=2) is the best choice for Ag+ $PtSe_2$+WS_2 based sensor configuration.

Later the importance of $PtSe_2$ is studied thoroughly in the structure configuration CaF_2+TiO_2+Ag/Au+ $PtSe_2$+graphene, which is represented in Fig 5. It is utmost visible that by the inclusion of a thin layer of $PtSe_2$ (4 nm), SPR curves are obtained at higher resonance angle with ultralow light reflectivity, which ensures higher sensitivity. $PtSe_2$ layer helps in enhancement of electric field

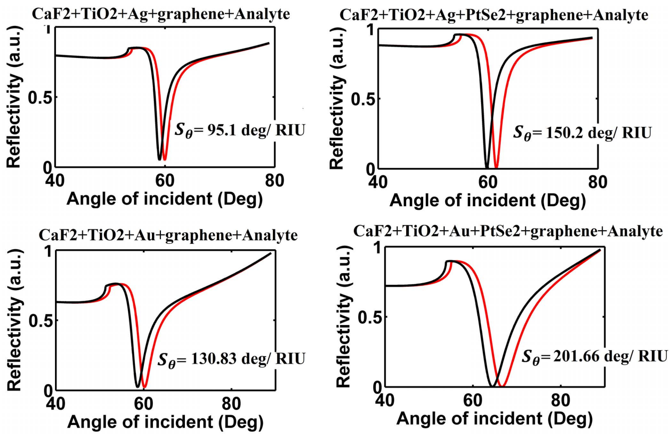

Fig. 5. Impact of $PtSe_2$ layer on the sensor performance.

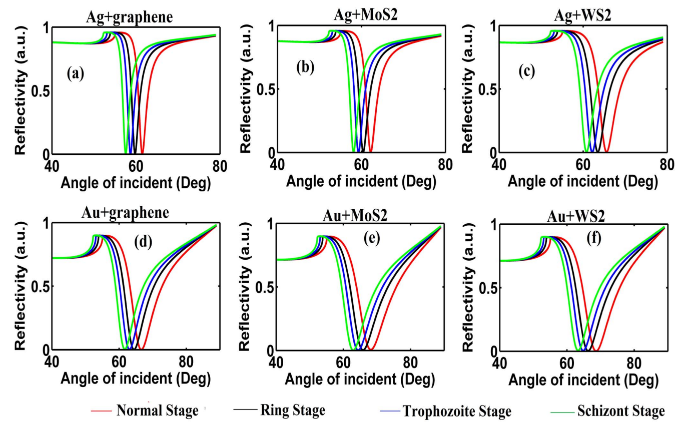

Fig. 6. Reflectance vs incident angle for different stages of malaria diseases at $d_{TiO_2} = 10nm$, $d_{Ag/Au} = 45nm$, $d_{PtSe_2} = 4nm$: (a)-(b) monolayer of graphene/MoS_2, (c) bilayer of WS_2, (d)-(f) monolayer of graphene/MoS_2/WS_2.

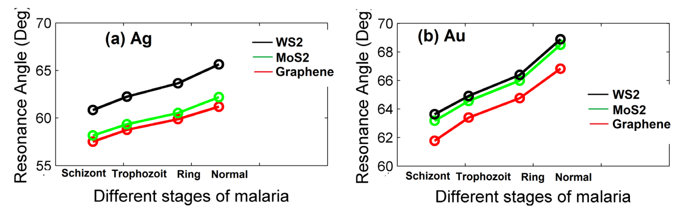

Fig. 7. Variation of resonance angle for different stages of malaria diseases.

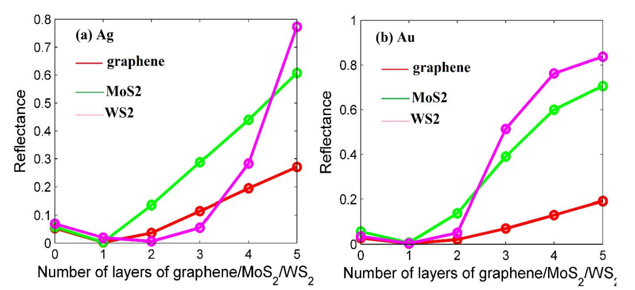

Fig. 8. Variation in reflectance intensity with respect to number of layers of graphene, MoS_2 and WS_2 for a fixed RI of the sensing medium of 1.408.

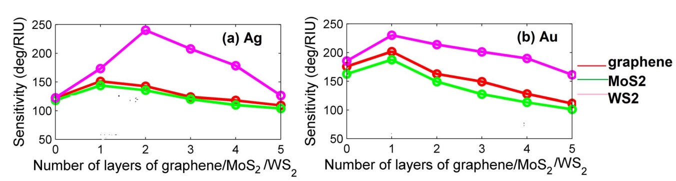

Fig. 9. Variation in sensitivity with respect to number of layers of graphene, MoS_2 and WS_2.

intensity which leads to more absorption of analytes in the sensing medium. It is seen that for Au+graphene based configuration, a sensitivity of 150.2°/RIU and 95.1 °/RIU is obtained with $PtSe_2$ and without $PtSe_2$ respectively. Similarly, for Au+graphene based structure a sensitivity of 201.66°/RIU and 130.83 °/RIU is obtained with $PtSe_2$ and without $PtSe_2$ respectively. Moreover, we have also investigated the effects of presence of $PtSe_2$ in combination with MoS_2 and WS_2, but not shown in the manuscript.

After optimizing the geometrical parameters of the proposed sensor, we studied the change in the reflectance characteristics with respect to the incident angle by infiltrating the sensing layer with blood analyte to detect various stages of malaria infection, which is delineated in Fig. 6. It is divulged that the SPR curves are moved to lower resonance angle and width of these curves become narrower as we infiltrated the blood with normal stage to ring stage to Trophozoite stage to Schizont stage of malaria. This decline nature of the resonance angle is because of the reduction in RI value from the normal stage to higher infectious stages of malaria diseases. It is noticed that higher resonance angles are obtained for the structure employing Au compared to the structure with Ag. Among graphene, MoS_2 and WS_2, it is observed that WS_2 shows SPR curves with more width and settles at higher resonance angle, which indicates higher sensing performance for WS_2 based proposed structure. The aforementioned statements are clearly verified in Fig. 7.

Upon increase in the number of layers of graphene/MoS_2/WS_2, we observed that the reflected light intensity increases, which is clearly visible in Fig. 8. It is revealed that for Ag based structure, the reflectance attains lowest value for L=1 for graphene and MoS_2, and a deviation is marked for WS_2 where reflectance is minimum for L=2. On the contrary, for Au based structural arrangement, minimum reflectance is accomplished for L=1 for graphene, MoS_2 and WS_2. So, for optimum sensing performance, it is advisable to design the sensor according to the aforementioned number of layers of graphene, MoS_2 and WS_2.

We analyzed the effect of number of layers of graphene, MoS_2 and WS_2 on the sensitivity, which is depicted in Fig. 9. It is seen that for Ag based configuration, maximum sensitivity of 150.99 °/RIU and 143.66°/RIU are observed at monolayer (L=1) of graphene and MoS_2 respectively, whereas optimum sensitivity of 240.10°/RIU is attained for bilayer (L=2) of WS_2. Similarly, it is found that for Au based configuration, optimum sensitivity of 201.66°/RIU, 187.5°/RIU and 230.19°/RIU are attained for monolayer (L=1) of graphene, MoS_2 and WS_2 respectively. It is also evident that for higher number of layers, sensitivity gradually decreases.

Fig. 10 represents the sensitivity variation of different malaria stages for Ag/Au metal layers employing graphene/MoS_2/WS_2. It can be perceived that maximum sensitivity is attained for the proposed structure using WS_2 compared to the graphene/MoS_2 based SPR sensor. An optimum sensitivity of 240.10 °/RIU and 230.19 °/RIU is realized for the structure configuration CaF_2/TiO_2/Ag/WS_2

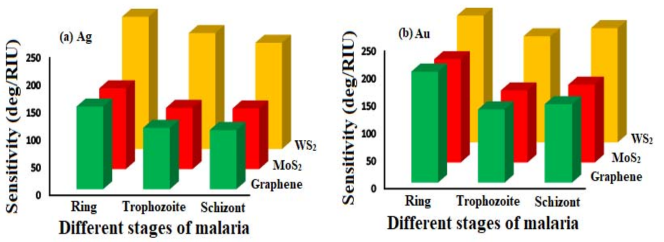

Fig. 10. Sensitivity analysis of the proposed (a) Ag (b) Au based structure.

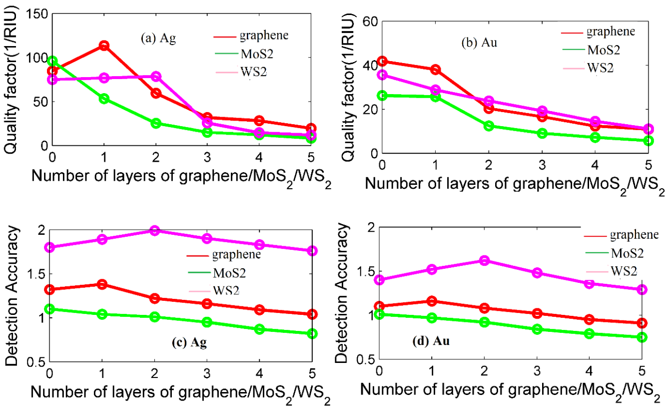

Fig. 11. Quality factor and detection accuracy of the proposed (a & c) Ag based and (b & d) Au based configurations.

(bilayer)/Analyte and $CaF_2/TiO_2/Au/WS_2$(monolayer)/Analyte respectively.

Next we computed other performance measuring parameters like quality factor and detection accuracy with respect to different number of layers (L) of 2D materials, which is shown in Fig. 11. It is clear that for Ag based structure, maximum Q and DA is attained for L=1 for graphene, L=0 for MoS_2 and L=2 for WS_2. On the other hand, for Au based configuration, maximum Q is achieved for L=0 for graphene, L=0 for MoS_2 and L=0 for WS_2, whereas, maximum DA is accomplished for L=1 for graphene, L=0 for MoS_2 and L=2 for WS_2. The aforementioned variations in Q and DA for different number of layers of 2D material is due to the dependency of these parameters on the FWHM of the SPR curves. It is worth mentioning that, absence of 2D materials (L=0) bestows better performance in some cases.

Additionally, we have employed the phase interrogation technique to observe the variation in phase with respect to the incident angle of the p-polarized light, which is represented in Fig. 12. Nevertheless we have performed the analysis for all the proposed configurations, but results of only WS_2 based configuration are shown here to simplify the manuscript. The upshots confirm an abrupt phase change between the incident and reflected light with a sharp slope. The position of the phase change is right-shifted as we infiltrated the sensing medium with blood having different stages of malaria infection i.e. from normal stage to schizont stage. More importantly, the phase change appears exactly at the same resonance angle as discussed in Fig. 6(c) and 6(f) for the proposed WS_2 based sensor configuration, which validates our outcomes. Moreover, the steep phase change indicates the ultrahigh sensitivity of the proposed sensor.

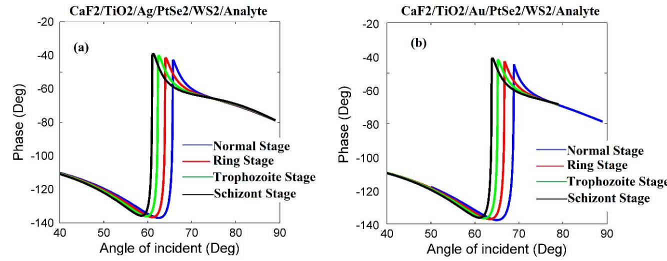

Fig. 12. Change in phase with respect to incident angle.

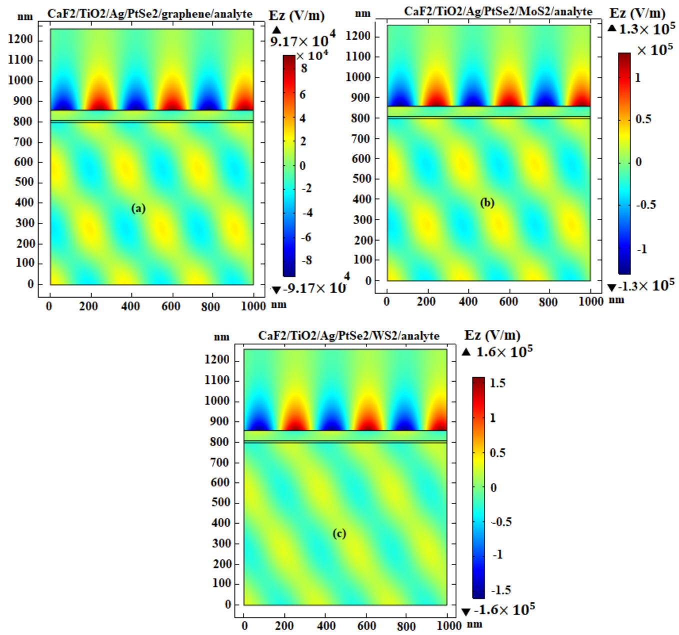

Fig. 13. Electric field distribution (a) Ag+graphene (b) Ag+MoS_2 (c) Ag+WS_2 configurations.

To analyse the sensing characteristics in a more proficient way, absorption behaviours of the proposed SPR configurations are scrutinized through surface plasmon electric field distribution by using COMSOL Multiphysics. Fig. 13 signifies the TM polarized electric fields for various proposed Ag based sensor configurations. It is shown that the incident p-polarized light stimulates the surface plasmon waves along the surface of different layers and finally the evanescent waves enters into the sensing layer. Also, it can be clearly perceived that WS_2 based sensor configuration delivers maximum field intensity as compared to graphene and MoS_2, which can be seen from the colorbar inserted in the figure. The sensing characteristics are envisaged by interaction of these evanescent waves with the blood analytes in the sensing medium.

Fig. 14 explains the change in field intensity along the metal-$PtSe_2$-WS_2 layers, where it can be observed that the electric fields are strongly localized near the $PtSe_2$ and WS_2 layer interface with a maximum intensity of $1.6 \times 10^5 V/m$ and $1.86 \times 10^5 V/m$ for Ag and Au based configuration respectively. Similar analysis is also carried out for graphene and MoS_2 based structure configurations, but not included in the manuscript to simplify the same. The electric fields are decayed in exponential manner towards the nearby sensing medium. Further, we have compared the field intensity in the presence of $PtSe_2$ and WS_2 with that of basic Kretschmann structure at the metal-sensing interface. An enhancement in

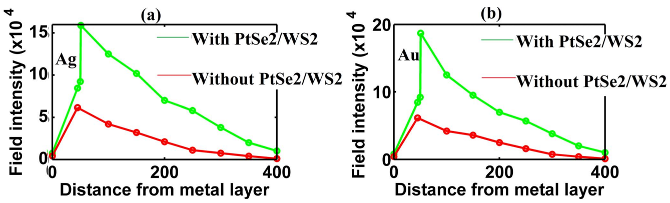

Fig. 14. Variation in electric field intensity from the metal layer surface (a) Ag (b) Au.

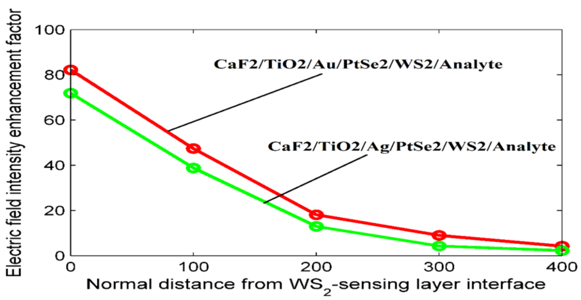

Fig. 15. Variation in EFIEF with respect to distance from the interface of WS_2-sensing medium for Ag and Au based proposed structure, for L=2 and sensing layer RI of 1.408.

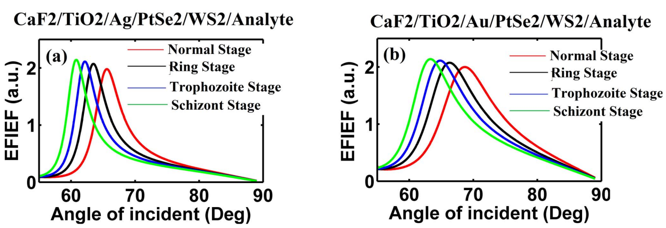

Fig. 16. EFIEF versus incident angle at $d_{TiO_2} = 10nm$, $d_{Ag/Au} = 45nm$, $d_{PtSe_2} = 4nm$, L=2 (Ag), L=1 (Au).

the electric field intensity can be clearly noticed with the inclusion of $PtSe_2$ and WS_2 on the metal layer, which boost the sensitivity of the sensor.

The electric field intensity enhancement factor (EFIEF) gives the extent of effective concentration of electric field in the vicinity of WS_2-sensing layer interface. EFIEF is defined as the ratio of square of the field $H_y(N/N-1)$ near the WS_2-sensing layer interface to the square of the field of $H_y(1/2)$ at the prism-metal interface, for the entering p-polarized signal. EFIEF at the interface of WS_2-sensing layer can be computed by involving both the electric and magnetic field, which is defined as [47],

$$\left|\frac{E_{\|}(N/N-1)}{E_{\|}(1/2}\right)\right|^2 = \frac{\varepsilon_1}{\varepsilon_N}\left|\frac{H_{y\|}(N/N-1)}{H_{y\|}(1/2}\right)\right|^2 \quad (16)$$

We computed the EFIEF in case of inclusion of different metal layers (Ag and Au), which is delineated in fig. 15. The EFIEF decreases exponentially with increase in distance from the WS_2-sensing layer interface, which indicates the proposed WS_2-based SPR sensor is extremely sensitive towards any small variation in the RI of sensing medium. Also, it can be perceived that the proposed Au and Ag based sensor configuration delivers a maximum value of EFIEF of 82.22 and 71.92 respectively. Therefore, with high value of EFIEF, Au-WS_2 based structure arrangement bestows higher sensitivity.

TABLE III
COMPARATIVE ANALYSIS OF SENSING PARAMETERS

References	Configurations	Sensitivity (°/RIU)	Q-factor (RIU^{-1})	DA
[12]	SF10/Au/MoS_2/graphene	87.80	17.56	1.28
[13]	SF10/ZnO/ Au/MoS_2/graphene	101.58	15.11	1.81
[26]	SF11/Ag/graphene/ MoS_2/TiO_2/SiO_2	98	88.88	0.88
[31]	BK7/ZnO/Si/MXene/Sensing layer	231	39.83	0.17
[25]	BK7/ZnO/Ag/$BaTiO_3$/WS_2	235	63.51	1.27
This work	CaF_2/TiO_2/Ag/$PtSe_2$/WS_2	240.10	78.46	1.99

Lastly, we assayed the variation of EFIEF for different stages of malaria diseases with respect to the incident angle for Ag based structure with bilayer of WS_2 and Au based configuration with monolayer of WS_2, which is shown in Fig. 16. It can be clearly observed that EFIEF attains the peak value exactly at the same resonance angle as explained in Fig. 6(c) and 6(f). Also, it is affirmed that maxima of EFIEF decreases as we infiltrate the sensing layer with blood cells with different stages of malaria diseases. At last, we compared the sensor performance with recently published theoretical works listed in the literature, which is summarized in Table III. From this table it can be clearly stated that our proposed sensor configuration delivers better performance compared to other related works.

IV. CONCLUSION

A novel Kretschmann configuration based SPR refractive index sensor is envisaged, which finds potential application in detection of various stages of malaria diseases. The proposed structure is analysed separately for Au and Ag as the metal layer, graphene/MoS_2/WS_2 as bioanalyte acknowledgment element and $PtSe_2$ as an intermediate layer to enhance the sensitivity. Thickness of metal layer, $PtSe_2$ layer and number layers of graphene, MoS_2 and WS_2 are sensibly optimized to maximize the sensor performance. Transfer matrix method is manipulated to simulate the proposed structures for analysis of angular reflectivity, whereas finite element method (computational background in COMSOL Multiphysics) is employed to study the TM polarized electric fields localization near the graphene/MoS_2/WS_2-sensing medium. Additionally, EFIEF is computed for the optimized sensor configuration. Finally, it is asserted that the Ag based SPR sensor employing bilayer (L=2) of WS_2 delivers remarkable sensing performance with a maximum sensitivity of 240.10 °/RIU, Q of 78.46 RIU^{-1} and DA of 1.99, whereas Au based structure employing monolayer (L=1) of WS_2 layer bestows superior sensing performance with a maximum sensitivity of 230.19 °/RIU, Q of 28.77 RIU^{-1} and DA of 1.54. The outcomes of the present work yield an innovative perspective in the field of the photonic sensors, which can be used for early stage detection of malaria diseases.

References

[1] H. H. Nguyen, J. Park, S. Kang, and M. Kim, "Surface plasmon resonance: A versatile technique for biosensor applications," *Sensors*, vol. 15, p. 10481, May 2015.

[2] H. Heidarzadeh, "Highly sensitive plasmonic sensor based on ring shape nanoparticles for the detection of ethanol and D-glucose concentration," *IEEE Trans. Nanotechnol.*, vol. 19, pp. 397–404, 2020.

[3] J. Zhou *et al.*, "Surface plasmon resonance (SPR) biosensors for food allergen detection in food matrices," *Biosensors Bioelectron.*, vol. 142, Oct. 2019, Art. no. 111449.

[4] B. D. Gupta, A. Pathak, and V. Semwal, "Carbon-based nanomaterials for plasmonic sensors: A review," *Sensors*, vol. 19, no. 16, p. 3536, Aug. 2019.

[5] N.-F. Chiu and H.-T. Yang, "High-sensitivity detection of the lung cancer biomarker CYFRA21-1 in serum samples using a carboxyl-MoS2 functional film for SPR-based immunosensors," *Frontiers Bioeng. Biotechnol.*, vol. 8, p. 234, Mar. 2020.

[6] S. A. Syubaev *et al.*, "Plasmonic nanolenses produced by cylindrical vector beam printing for sensing applications," *Sci. Rep.*, vol. 9, no. 1, p. 19750, Dec. 2019.

[7] S. Agarwal, P. Giri, Y. K. Prajapati, and P. Chakrabarti, "Effect of surface roughness on the performance of optical SPR sensor for sucrose detection: Fabrication, characterization, and simulation study," *IEEE Sensors J.*, vol. 16, no. 24, pp. 8865–8873, Dec. 2016.

[8] S. Pal, Y. K. Prajapati, and J. P. Saini, "Influence of graphene's chemical potential on SPR biosensor using ZnO for DNA hybridization," *Opt. Rev.*, vol. 27, no. 1, pp. 57–64, Feb. 2020.

[9] R. Jha and A. K. Sharma, "High-performance sensor based on surface plasmon resonance with chalcogenide prism and aluminum for detection in infrared," *Opt. Lett.*, vol. 34, no. 6, p. 749, Mar. 2009.

[10] W. Su, G. Zheng, and X. Li, "Design of a highly sensitive surface plasmon resonance sensor using aluminum-based diffraction grating," *Opt. Commun.*, vol. 285, nos. 21–22, pp. 4603–4607, Oct. 2012.

[11] X. Sang and D. Zhang, "Research on the SPR properties of copper thin film with regulation of titanium dioxide," *Spectroscopy Spectr. Anal.*, vol. 36, no. 7, pp. 2027–2030, 2016.

[12] M. S. Rahman, M. S. Anower, M. R. Hasan, M. B. Hossain, and M. I. Haque, "Design and numerical analysis of highly sensitive Au-MoS2-graphene based hybrid surface plasmon resonance biosensor," *Opt. Commun.*, vol. 396, pp. 36–43, Aug. 2017.

[13] A. S. Kushwaha, A. Kumar, R. Kumar, and S. K. Srivastava, "A study of surface plasmon resonance (SPR) based biosensor with improved sensitivity," *Photon. Nanostruct. Fundamentals Appl.*, vol. 31, pp. 99–106, Sep. 2018.

[14] A. K. Geim, "Graphene: Status and prospects," *Science*, vol. 324, pp. 1530–1534, Jun. 2009.

[15] F. Bonaccorso, Z. Sun, T. Hasan, and A. C. Ferrari, "Graphene photonics and optoelectronics," *Nature Photon.*, vol. 4, no. 9, pp. 611–622, Sep. 2010.

[16] M. Kukkar *et al.*, "Application of MoS2 modified screen printed electrodes for highly sensitive detection of bovineserum albumin," *Analytica Chimica Acta*, vol. 939, pp. 101–107, Oct. 2016.

[17] L. Yuan and L. Huang, "Exciton dynamics and annihilation in WS2 2D semiconductors," *Nanoscale*, vol. 7, no. 16, p. 7402, 2015.

[18] B. Zhu, X. Chen, and X. Cui, "Exciton binding energy of monolayer WS2," *Sci. Rep.*, vol. 5, no. 1, p. 9218, Aug. 2015.

[19] Y. Wang *et al.*, "Monolayer $PtSe_2$, a new semiconducting transition-metal-dichalcogenide, epitaxially grown by direct selenization of Pt," *Nano Lett.*, vol. 15, no. 6, pp. 4013–4018, Jun. 2015.

[20] Y. Zhao *et al.*, "High-electron-mobility and air-stable 2D layered $PtSe_2$ FETs," *Adv Mater.*, vol. 29, Feb. 2017, Art. no. 1604230.

[21] E. Gao, S.-Z. Lin, Z. Qin, M. J. Buehler, X.-Q. Feng, and Z. Xu, "Mechanical exfoliation of two-dimensional materials," *J. Mech. Phys. Solids*, vol. 115, pp. 248–262, Jun. 2018.

[22] H. G. Kim and H.-B.-R. Lee, "Atomic layer deposition on 2D materials," *Chem. Mater.*, vol. 29, no. 9, pp. 3809–3826, Apr. 2017.

[23] Y. Liu, S. Zhang, J. He, Z. M. Wang, and Z. Liu, "Recent progress in the fabrication, properties, and devices of heterostructures based on 2D materials," *Nano-Micro Lett.*, vol. 11, no. 1, p. 13, Dec. 2019.

[24] L. Tang, J. Tan, H. Nong, B. Liu, and H.-M. Cheng, "Chemical vapor deposition growth of two-dimensional compound materials: Controllability, material quality, and growth mechanism," *Accounts Mater. Res.*, vol. 2, no. 1, pp. 36–47, Jan. 2021.

[25] A. Kumar, A. K. Yadav, A. S. Kushwaha, and S. K. Srivastava, "A comparative study among WS2, MoS2 and graphene based surface plasmon resonance (SPR) sensor," *Sens. Actuators Rep.*, vol. 2, no. 1, Nov. 2020, Art. no. 100015.

[26] M. Moznuzzaman, M. R. Islam, M. B. Hossain, and I. M. Mehedi, "Modeling of highly improved SPR sensor for formalin detection," *Results Phys.*, vol. 16, Mar. 2020, Art. no. 102874.

[27] D. T. Nurrohman and N.-F. Chiu, "Surface plasmon resonance biosensor performance analysis on 2D material based on graphene and transition metal dichalcogenides," *ECS J. Solid State Sci. Technol.*, vol. 9, no. 11, Jan. 2020, Art. no. 115023.

[28] R. Kumar, A. S. Kushwaha, M. Srivastava, H. Mishra, and S. K. Srivastava, "Enhancement in sensitivity of graphene-based zinc oxide assisted bimetallic surface plasmon resonance (SPR) biosensor," *Appl. Phys. A, Solids Surf.*, vol. 124, no. 3, p. 235, Mar. 2018.

[29] A. Panda, P. D. Pukhrambam, and G. Keiser, "Performance analysis of graphene-based surface plasmon resonance biosensor for blood glucose and gas detection," *Appl. Phys. A, Solids Surf.*, vol. 126, no. 3, p. 153, Mar. 2020.

[30] M. Wang *et al.*, "Theoretical design of a surface plasmon resonance sensor with high sensitivity and high resolution based on graphene–WS2 hybrid nanostructures and Au-Ag bimetallic film," *RSC Adv.*, vol. 7, no.75, p. 47177, 2017.

[31] R. Kumar, S. Pal, Y. K. Prajapati, and J. P. Saini, "Sensitivity enhancement of MXene based SPR sensor using silicon: Theoretical analysis," *Silicon*, vol. 13, no. 6, pp. 1887–1894, Jun. 2021.

[32] K. V. Sreekanth *et al.*, "Extreme sensitivity biosensing platform based on hyperbolic metamaterials," *Nature Mater.*, vol. 15, no. 6, pp. 621–627, Jun. 2016.

[33] K. V. Sreekanth *et al.*, "Extreme sensitivity biosensing platform based on hyperbolic metamaterials," *Adv. Opt. Mat.*, vol. 4, pp. 1767–1772, Jun. 2016.

[34] K. V. Sreekanth *et al.*, "Hyperbolic metamaterials-based plasmonic biosensor for fluid biopsy with single molecule sensitivity," *EPJ Appl. Metamater.*, vol. 4, p. 1, Feb. 2017, Art. no. 4.

[35] A. V. Kabashin *et al.*, "Plasmonic nanorod metamaterials for biosensing," *Nature Mater.*, vol. 8, no. 11, pp. 867–871, Nov. 2009.

[36] D. Garoli, E. Calandrini, G. Giovannini, A. Hubarevich, V. Caligiuri, and F. D. Angelis, "Nanoporous gold metamaterials for high sensitivity plasmonic sensing," *Nanosc. Horizons*, vol. 4, no. 5, pp. 1153–1157, Aug. 2019.

[37] E. Calandrini *et al.*, "3D nanoporous antennas as a platform for high sensitivity IR plasmonic sensing," *Opt. Exp.*, vol. 27, pp. 25912–25919, Sep. 2019.

[38] Ankita, B. Suthar, and A. Bhargava, "Biosensor application of one-dimensional photonic crystal for malaria diagnosis," *Plasmonics*, vol. 16, no. 1, pp. 59–63, Feb. 2021.

[39] T. Noppadon, D. Chatnapa, and W. K. P. Srivicha, "Malaria diagnosis, a brief review," *Korean J. Parasitol.*, vol. 47, no. 2, pp. 93–102, 2009.

[40] M. Agnero *et al.*, "Malaria-infected red blood cell analysis through optical and biochemical parameters using the transport of intensity equation and the microscope's optical properties," *Sensors*, vol. 19, no. 14, p. 3045, Jul. 2019.

[41] N.-F. Chiu, Y.-C. Tu, and T.-Y. Huang, "Enhanced sensitivity of anti-symmetrically structured surface plasmon resonance sensors with zinc oxide intermediate layers," *Sensors*, vol. 14, pp. 87–170, Jan. 2013.

[42] G. T. West, P. J. Kelly, and J. W. Bradley, "A comparison of thin silver films grown onto zinc oxide via conventional magnetron sputtering and HiPIMS deposition," *IEEE Trans. Plasma Sci.*, vol. 38, no. 11, pp. 3057–3061, Nov. 2010.

[43] H. Aouani *et al.*, "Crucial role of the adhesion layer on the plasmonic fluorescence enhancement," *ACS Nano*, vol. 3, no. 7, pp. 2043–2048, 2009.

[44] L. Han, X. Zhao, T. Huang, H. Ding, and C. Wu, "Comprehensive study of phase-sensitive SPR sensor based on metal–ITO hybrid multilayer," *Plasmonics*, vol. 14, no. 6, pp. 1743–1750, Dec. 2019.

[45] S. Gan, H. Wang, J. Liang, X. Dai, and Y. Xiang, "Ultra-sensitive refractive index sensors based on bloch surface waves with transition metal dichalcogenides," *IEEE Sensors J.*, vol. 19, no. 19, pp. 8675–8680, Oct. 2019.

[46] V. G. Kravets, "Ellipsometry and optical spectroscopy of low-dimensional family TMDs," *Semicond. Phys. Quantum Electron. Optoelectronics*, vol. 20, no. 3, pp. 284–296, Oct. 2017.

[47] P. K. Maharana, R. Jha, and P. Padhy, "On the electric field enhancement and performance of SPR gas sensor based on graphene for visible and near infrared," *Sens. Actuators B, Chem.*, vol. 207, pp. 117–122, Feb. 2015.